

Nanoscale

Accepted Manuscript



This is an *Accepted Manuscript*, which has been through the Royal Society of Chemistry peer review process and has been accepted for publication.

Accepted Manuscripts are published online shortly after acceptance, before technical editing, formatting and proof reading. Using this free service, authors can make their results available to the community, in citable form, before we publish the edited article. We will replace this *Accepted Manuscript* with the edited and formatted *Advance Article* as soon as it is available.

You can find more information about *Accepted Manuscripts* in the [Information for Authors](#).

Please note that technical editing may introduce minor changes to the text and/or graphics, which may alter content. The journal's standard [Terms & Conditions](#) and the [Ethical guidelines](#) still apply. In no event shall the Royal Society of Chemistry be held responsible for any errors or omissions in this *Accepted Manuscript* or any consequences arising from the use of any information it contains.

Cite this: DOI: 10.1039/c0xx00000x

www.rsc.org/xxxxxx

REVIEW

Electrical Spin Injection and Transport in Semiconductor Nanowires: Challenges, Progress and Perspectives

Jianshi Tang,^{*ab} and Kang L. Wang^{*a}*Received (in XXX, XXX) Xth XXXXXXXXX 20XX, Accepted Xth XXXXXXXXX 20XX*

DOI: 10.1039/b000000x

Spintronic devices are of fundamental interest for their nonvolatility and great potential for low-power electronic applications. The implementation of those devices usually favors materials with long spin lifetime and spin diffusion length. Recent spin transport studies in semiconductor nanowires have shown much longer spin lifetimes and spin diffusion lengths than those reported in bulk/thin films. In this paper, we will review recent progress in the electrical spin injection and transport in semiconductor nanowires and draw a comparison with that in bulk/thin films. In particular, the challenges and methods of making high-quality ferromagnetic tunneling and Schottky contacts on semiconductor nanowires as well as thin films will be discussed. Besides, commonly used methods for characterizing spin transport will be introduced, and their applicability in nanowire devices will be discussed. Moreover, the effect of spin-orbit interaction strength and dimensionality on the spin relaxation and hence the spin lifetime will be investigated. Finally, for further device applications, we will examine several proposals of spinFETs and provide a perspective of future studies on semiconductor spintronics.

1. Introduction

In the efforts to reduce the power dissipation and variability in the continuous scaling of Si technology,¹ spin-based electronics (spintronics) has emerged as an appealing solution, which utilizes both charge and spin of the electron for information processing.²⁻³ Since the discovery of the giant magnetoresistance (GMR) effect in the 1980s,⁴⁻⁵ numerous efforts have been devoted to study the spin transport in various metals and semiconductors, including Cu,⁶ Al,⁷ Si,⁸⁻⁹ Ge,¹⁰⁻¹¹ GaAs,¹²⁻¹³ and graphene.¹⁴⁻¹⁵ Furthermore, several variants of spin field-effect transistor (spinFET) have been proposed as an attractive candidate to substitute the traditional charge-based Si metal-oxide-semiconductor (MOS) transistor for low-power applications.¹⁶⁻²⁰ A typical spinFET consists of a semiconductor channel with two ferromagnetic contacts, whose relative magnetization orientation modulates the transistor's current drivability. The operation of spinFETs usually involves the injection, manipulation and detection of electron spins in the charge/spin transport process. SpinFETs are expected to provide unique advantages of low power dissipation and increased functionalities because of their nonvolatility nature and additional control of the current from the ferromagnetic state other than the gate electrode. In order to realize most spintronic devices, it is essential to achieve efficient spin injection into semiconductors and further to effectively manipulate the spin transport in them. For this purpose, the electrical spin injection and transport in a broad range of semiconductors have been extensively studied to find materials with long spin lifetime and diffusion length.⁹⁻¹⁵ In the literature, most pioneer work has been conducted on bulk and thin film semiconductors, because they are easy to tune the doping profile and fabricate into devices. Si and Ge are of particular interest due to their easy integration into current CMOS technology in the future. The observed spin

lifetime ranges from tens of picoseconds to several nanoseconds, and the diffusion length is typically hundreds of nanometers (see **Table 1** later).

Recently, several works on spin injection into semiconductor nanowires revealed a longer spin lifetime and diffusion length compared with their bulk/thin film counterparts.¹⁹⁻²⁵ Theoretical studies also suggested that the spin relaxation can be significantly suppressed in quasi-one-dimensional (1-D) nanostructures.²⁶ This raises great interest to study the electrical spin injection and transport in nanostructures. Hereby, in this paper, we will review recent progress in the spin transport studies in semiconductor nanostructures, mainly focusing on Ge/Si nanowires. This review paper is structured as follows: we will first discuss several important issues in the material preparation for spin injection studies, followed by introducing commonly used methods for characterizing spin transport. The literature results of spin lifetime and spin diffusion length in several bulk/thin film semiconductors will also be presented in this part. Then we will review recent progress of spin injection and transport studies in semiconductor nanostructures, mainly focusing on nanowires. Experimental results for both tunneling and Schottky contact spin injection into semiconductor nanowires will be highlighted. In particular, the issues of fabricating high-quality ferromagnetic contacts on nanowires considering their unique 1-D geometry will be discussed. We will also compare the spin lifetime and spin diffusion length values in nanowires with those reported for bulk and thin films. Finally, we will recap several proposals of spinFETs and provide a perspective of future studies on semiconductor spintronics.

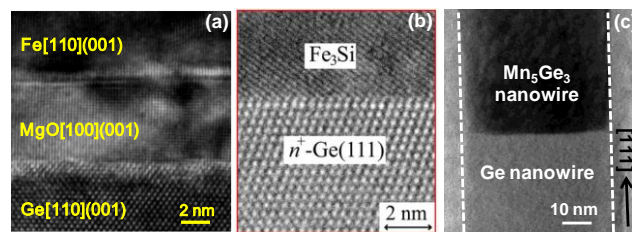
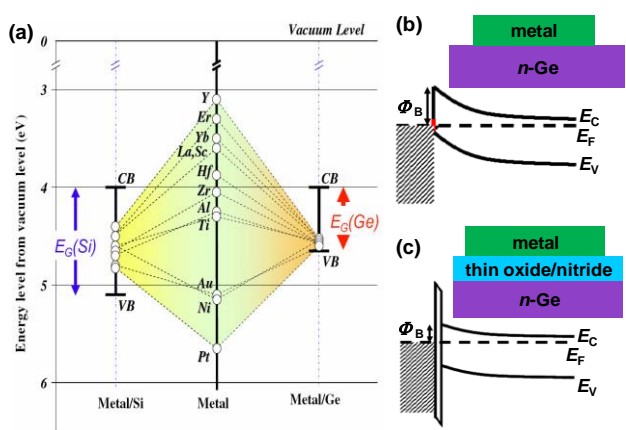


Fig. 2: Ferromagnetic contacts with atomically clean interfaces for electrical spin injection. (a) TEM image of an epitaxial Fe/MgO/Ge tunnel junction grown by MBE. Reproduced with permission from Ref. [30]. Copyright 2009, Elsevier. (b) TEM image of an epitaxial Fe₃Si/Ge Schottky junction grown by low-temperature MBE. Reproduced with permission from Ref. [43]. Copyright 2012, AIP Publishing LLC. (c) TEM image of a Mn₅Ge₃/Ge nanowire heterostructure fabricated by RTA at 450 °C. Reproduced with permission from Ref. [47]. Copyright 2012, American Chemical Society. All of these structures for electrical spin injection maintain atomically smooth interfaces to minimize interface states.

Fig. 1: Fermi level pinning issue in metal/semiconductor contact. (a) Schottky barrier heights for various metal/Si and metal/Ge contacts with different metal work functions. In the case of Ge, the Fermi level is strongly pinned close to the Ge valence band edge. Reproduced with permission from Ref. [33]. Copyright 2009, Elsevier. Schematics of the band diagram of (b) a strongly pinned Ge Schottky contact (Fermi level pinned at the charge-neutrality point) and (c) a pinning-alleviated Ge contact by insertion of a thin tunneling oxide/nitride. Reproduced with permission from Ref. [37]. Copyright 2008, AIP Publishing LLC.

2. Electrical spin transport in semiconductor bulk and thin films

2.1. Material preparation for electrical spin injection

As discussed above, successful spin injection into semiconductors is one of the key steps to demonstrate many novel spintronic devices. However, while the electrical spin injection into ordinary metals can be readily demonstrated in metallic spin valve structures,⁶⁻⁷ the realization of efficient spin injection into semiconductors is much complicated by several factors: 1) the large conductivity difference between ordinary ferromagnetic metals (FM) and semiconductors (SC) would make the spin injection efficiency negligibly small, which is well known as the conductivity mismatch problem;²⁷ 2) the increase in the doping concentration of the semiconductor channel in order to reduce such a conductivity difference, however, would decrease the spin lifetime due to the aggravated spin relaxation from impurity scatterings;³ 3) while the insertion of a tunneling or Schottky barrier helps alleviate the conductivity mismatch problem,²⁸⁻²⁹ the preparation of a high-quality tunneling oxide without pinholes or a defect-free Schottky contact without Fermi-level pinning is not trivial.³⁰⁻³¹ Moreover, the localized states at the FM/SC interface and the surface roughness could significantly complicate and jeopardize the spin injection process.³² It is also worth noting that the interface states would induce Fermi level pinning in typical metal/semiconductor contacts. For example, the Fermi level in conventional metal/Ge contacts is strongly pinned close to the Ge valence band edge due to a high density of interface states, as shown in **Fig. 1(a)**.³³ Even for Si with a lower density of interface states, the ideal Schottky-Mott limit is hardly observed.

In order to alleviate the Fermi level pinning in metal/semiconductor contacts, inserting a thin intervening insulator is an effective approach to modulate the Schottky barrier height. As illustrated in **Figs. 1(b-c)**, the thin insulator layer is considered either to passivate the semiconductor surface states and/or to reduce the metal-induced gap states by

suppressing the wave function tailing of the metal into the band gap of the semiconductor.³⁴ Experimentally, various insulators, including Ge₃N₄,³⁵ GeO_x,³⁶ Al₂O₃,³⁷ and MgO,³⁸ deposited by plasma nitridation, sputtering, electron beam evaporation, or molecular beam epitaxy (MBE), have been studied as the intervening layer to effectively depin the Fermi level in metal/Ge contacts. Among those deposition methods, the epitaxial growth of MgO using MBE is considered as the one of the best options for Ge because the single-crystalline and atomically smooth MgO can be grown epitaxially on Ge, in which the MgO thickness and epitaxial relationship can be precisely controlled (see **Fig. 2(a)**).³⁰ Moreover, the epitaxial Fe/MgO/Ge tunnel junction possesses a unique 45 degree rotation between the MgO and Ge lattices to minimize the lattice mismatch of the two and to enhance the spin filtering.³⁹ Indeed, the first nonlocal electrical spin injection and transport in Ge was demonstrated using epitaxial Fe/MgO/Ge tunnel junctions, which will be discussed later.¹⁰ Besides to MgO, native oxides (SiO₂ and GeO_x) and Al₂O₃ (usually by oxidizing a thin layer of Al) are also widely used as the tunneling oxide in the spin injection into Si and Ge.^{9-11, 40-42}

On the other hand, direct deposition of ferromagnetic contacts with Schottky barriers have also been attempted on semiconductors for spin transport studies. Here it is very important to maintain atomically smooth interface for the FM/SC Schottky contacts to minimize defects-induced interface states and Fermi level pinning.³¹ Recently, MBE epitaxial growth has been demonstrated to grow single-crystalline silicide contacts on Ge/Si with atomically smooth interfaces, as shown in **Fig. 2(b)**.⁴³ Besides to the epitaxial growth, although it is possible to form ferromagnetic germanide/silicide contacts in a standard germanidation/silicidation process, it is very difficult to maintain high-quality interfaces with bulk Ge/Si. For Ge/Si nanowires, however, the 1-D germanidation/silicidation with rapid thermal annealing (RTA) has been extensively studied to produce single-crystalline germanide/silicide contacts with atomically clean interfaces.^{22, 44-47} For example, **Fig. 2(c)** shows the transmission electron microscope (TEM) image of a Mn₅Ge₃/Ge nanowire heterostructure fabricated by the solid-state reaction between a Ge nanowire and Mn metal contacts upon RTA at 450 °C.⁴⁷ We will discuss more in the Section 3.3 of Ge/Si nanowires.

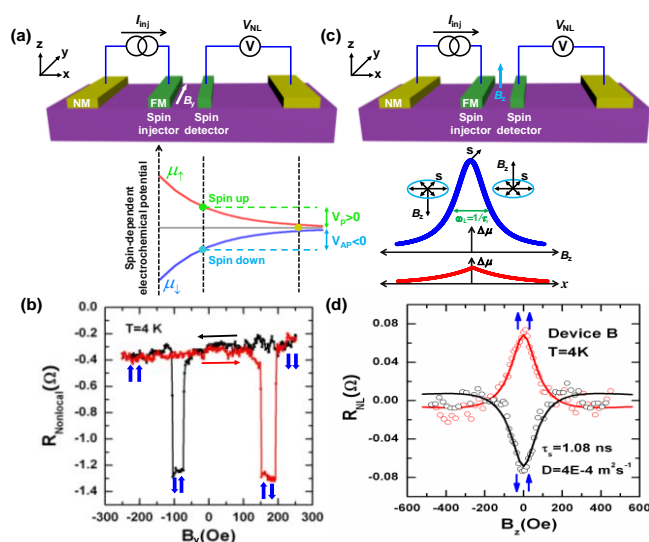


Fig. 3: Nonlocal spin valve and Hanle measurements. (a) Schematic illustration of nonlocal spin valve measurement in which an in-plane magnetic field is applied along the easy axis of the ferromagnetic spin injector and detector. (b) Typical nonlocal spin valve signal measured in n -Ge at 4 K. The black and red arrows indicate the sweeping direction of the magnetic field. The blue arrows indicate the relative magnetization directions of the spin injector and detector. (c) Schematic illustration of nonlocal Hanle measurement in which an out-of-plane magnetic field is applied perpendicular to the FM/SC interface. (d) Typical nonlocal Hanle precession signal measured in n -Ge at 4 K. (b) and (d) are reproduced with permission from Ref. [10] Copyright 2011 by the American Physical Society.

2.2. Electrical characterization of spin transport

Spin injection and transport is usually electrically characterized by nonlocal spin valve and Hanle precession measurements, from which the spin lifetime and spin diffusion length can be extracted.^{6-7, 9-10} Likewise, optical detection of the spin injection has also been reported in a Si n - i - p spinLED structure with an Fe/Al₂O₃ ferromagnetic tunneling contact by detecting the emitted polarized light.⁸ Here we only focus on the electrical detection in this review paper. In the nonlocal spin valve measurement as illustrated in Fig. 3(a), a spin-polarized current is injected from a ferromagnetic contact (spin injector) to create a spin accumulation in the semiconductor channel, while another ferromagnetic contact (spin detector), placed outside the charge current loop, probes the spin-dependent electrochemical potential of one spin channel (spin up or down) in relation to the reference contact. As the relative magnetization direction of the spin injector and the detector switches from parallel state to anti-parallel state by the in-plane magnetic field, a bipolar nonlocal voltage V_{NL} should be sensed, namely $V_p > 0$ and $V_{AP} < 0$ in the ideal case. Fig. 3(b) shows an example of typical nonlocal spin valve signals measured from Ge.¹⁰ In this measurement, the spin potential (voltage) sense loop is separated from the current loop to avoid any suspicious artifacts; therefore, nonlocal spin valve signal is usually considered as a clear evidence for successful spin injection.

Theoretically, in the tunneling contact spin injection case where the tunnel barrier resistance is typically much larger than the channel resistance over a spin diffusion length ($R_N = \lambda_{sf}/\sigma_s A$), the nonlocal spin valve signal can be derived from the 1-D spin drift-diffusion model as:⁷

$$\frac{V_{NL}}{I_{inj}} = \pm \frac{1}{2} P_J^2 \frac{\lambda_{sf}}{\sigma_s A} \exp\left(-\frac{L}{\lambda_{sf}}\right) \quad (1)$$

where P_J is the spin polarization of the current I_{inj} injected from the spin injector into the semiconductor channel, λ_{sf} is the spin diffusion length, σ_s is the semiconductor conductivity, A is the semiconductor channel cross-sectional area, and L is the spatial distance between the spin injector and detector. The $+(-)$ sign denotes the parallel (anti-parallel) magnetization state for the spin injector and detector. In experiments, there is typically a nonzero background voltage on the measured V_{NL} ,⁴⁸ and the total change in the nonlocal spin valve signal is usually measured for further physical interpretation (such as the extraction of the spin diffusion length), and it is given by:

$$\Delta R_{NL} = \frac{|V_p - V_{AP}|}{I_{inj}} = P_J^2 \frac{\lambda_{sf}}{\sigma_s A} \exp\left(-\frac{L}{\lambda_{sf}}\right) \quad (2)$$

which is a simple exponential decay function of the spatial distance L with respect to the spin diffusion length λ_{sf} (typically hundreds of nanometers as shown in Table 1 later). It also suggests that, in order to observe appreciable nonlocal spin valve signal, the designed distance between the spin injector and detector in practical devices is required to be at most comparable with the spin diffusion length, and hence high-resolution e-beam lithography is usually adopted in the device fabrication.

Unlike the nonlocal spin valve measurement with in-plane field, in the Hanle effect measurement, an out-of-plane magnetic field is applied to induce the spin precession about the magnetic field direction, as shown in Fig. 3(c).⁹ Hanle measurements can be performed in both three-terminal (3-T, usually referred as “local”) and four-terminal (4-T, referred to as “nonlocal” or “NL”) device structure. However, the latter is usually adopted to avoid any spurious signals and to provide a conclusive evidence for successful spin injection.⁴⁹ In the 4-T configuration, the spin injector and the spin detector are spatially separated so that the spin signal sense loop is separated from the charge current loop (similar to the nonlocal spin valve device), compared with the 3-T configuration in which the spin injector and detector are the same ferromagnetic contact. Theoretically, the precession and dephasing of the injected spins as a function of the magnetic field can be described using the 1-D spin drift-diffusion model:⁷

$$\frac{V_{NL}}{I_{inj}} = \pm P_J^2 \frac{D}{\sigma_s A} \int_0^\infty \frac{1}{\sqrt{4\pi Dt}} \exp\left(-\frac{L^2}{4Dt}\right) \cos(\omega_L t) \exp\left(-\frac{t}{\tau_s}\right) dt \quad (3)$$

where D is the diffusion constant, τ_s is the spin lifetime, and $\omega_L = g\mu_B B_z/\hbar$ is the Larmor frequency (g is the Landé g -factor of the electron, μ_B is the Bohr magneton, B_z is the out-of-plane magnetic field, \hbar is the reduced Planck constant). Again, the $+(-)$ sign denotes the parallel (anti-parallel) magnetization state for the spin injector and detector. D and τ_s can be obtained by numerical fitting of the Hanle curve, and then the spin diffusion length can be calculated as $\lambda_{sf} = \sqrt{D\tau_s}$. Under certain circumstance (especially for the 3-T device geometry where the dimension of the ferromagnetic contact is typically much larger than the spin diffusion length), the Hanle curve can be approximately represented by a Lorentzian function:

$$V_{NL} = V_0/[1 + (\omega_L \tau_s)^2] \quad (4)$$

Fig. 3(d) shows an example of typical nonlocal Hanle curves

Cite this: DOI: 10.1039/c0xx00000x

www.rsc.org/xxxxxxx

REVIEW

Table 1. Typical spin lifetime and spin diffusion length in Ge/Si bulk and thin films

SC	n or p (cm ⁻³)	FM	Barriers	Methods	T (K)	τ_{sf} (ns)	λ_{sf} (μ m)	Ref.
<i>i</i> -Si	undoped	Co ₈₄ Fe ₁₆	Schottky	Hot e^-	85	1	N/A	[50]
<i>n</i> -Si	5×10^{19}	Fe	Al ₂ O ₃	NL	10	0.9	0.95	[51]
	5×10^{19}	Fe	MgO	NL/3-T	8	8.95/8.50	1.72/1.68	[52]
	3×10^{18}	Ni ₈₀ Fe ₂₀	SiO ₂	3-T	10	0.32	0.19	[53]
	1×10^{19}	Ni ₈₀ Fe ₂₀	Graphene	3-T	4	0.14	0.12	[54]
	1.8×10^{19}	Ni ₈₀ Fe ₂₀	Al ₂ O ₃	3-T	300	0.14	0.23	[9]
	6×10^{17}	CoFe	Schottky	3-T	300/40	1.36/3.02	N/A	[55]
<i>p</i> -Si	4.8×10^{18}	Ni ₈₀ Fe ₂₀	Al ₂ O ₃	3-T	300	0.27	0.31	[9]
<i>p</i> -Ge	8.2×10^{18}	Fe	MgO	3-T	300	0.013	0.08	[41]
<i>n</i> -Ge	2×10^{19}	Fe	MgO	NL	4	1.08	0.58	[10]
	2.5×10^{18}	CoFe	MgO	3-T	300	0.12	0.683	[11]
	10^{18} - 10^{19}	Ni ₈₀ Fe ₂₀	Al ₂ O ₃	3-T	10	0.035	N/A	[56]
	10^{18}	Fe	Schottky	3-T	50	0.14	0.63	[43]

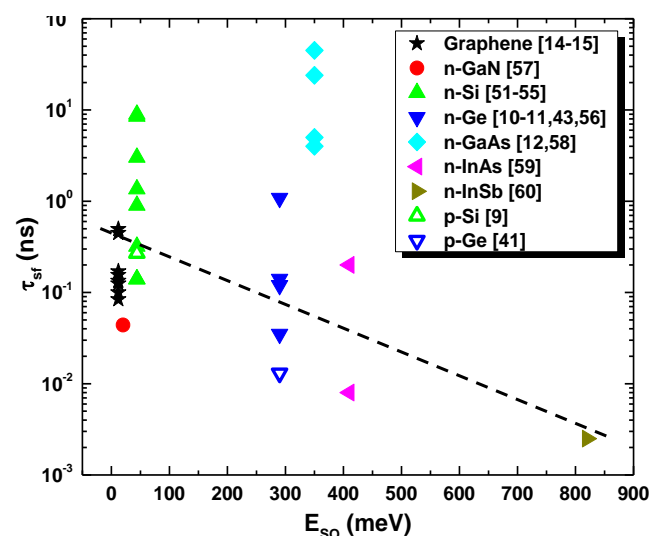


Fig. 4: SOI effect on the spin lifetime in semiconductors. Literature-reported spin lifetimes in various semiconductors as a function of the SOI strength represented by the spin-orbit splitting energy E_{SO} . The dash line is a guide to the eye: stronger SOI generally leads to smaller spin lifetime.

measured from Ge.¹⁰ Besides, it is worth mentioning that also inverted Hanle effect measurements are reported as an important evidence for successful spin injection,³² especially for 3-T device configuration. Different from the normal Hanle measurement, the magnetic field in the inverted Hanle measurement is applied in plane, which effectively suppresses the spin precession and increases the spin accumulation. Therefore, the measured inverted Hanle signal looks like a upside-down (so-called “inverted”) Lorentzian function.³²

2.3. Spin lifetime and spin diffusion length in bulk Ge/Si

In literature, there have been extensive studies on the spin

lifetime and spin diffusion length in both *n*- and *p*-type Ge/Si under a wide range of conditions, including doping concentrations from intrinsic to degenerate level, temperatures from liquid helium temperature to room temperature and even up to 500 K, with different ferromagnets and barriers (tunnel oxides and Schottky barriers). Most experiments are carried out in 3-T geometry rather than 4-T, mainly because the former one benefits from its simple device fabrication process with convenient photolithography rather than electron-beam lithography. For bulk Si/Ge with crystal inversion symmetry, the spin relaxation is dominated by the Elliott-Yafet mechanism, in which the spin relaxation is accompanied by momentum scattering (by phonons and impurities) through the spin-orbit interaction (SOI).³ **Table 1** lists selected literature results of spin lifetime and spin diffusion length for Ge/Si bulk and thin films.^{9-11, 41, 43, 50-56} A broader literature survey of spin lifetime specifically in *n*-type Si can be found in Ref. [48].⁴⁸

It is noted that there is a considerable discrepancy among the values obtained by different research groups. This is because the spin injection process is very sensitive to the FM/SC interface, including the surface roughness and interface states, which is closely related to how the FM/SC junction is prepared. Also, different measurement methods (3-T versus 4-T) could also give very different results, arising from the surface roughness-induced magnetostatic fields and the bias effect on the spin transport process.^{32, 49} In general, Si is found to have a relatively longer spin lifetime compared with Ge, which is because Si ($E_{SO} = 0.044$ eV) has a much weaker SOI than Ge ($E_{SO} = 0.29$ eV).

To get a better understanding of the spin lifetime dependence on the SOI, we plot the measured spin lifetime of Ge/Si as a function of the SOI strength represented by the spin-orbit splitting energy (E_{SO}), as shown in **Fig. 4**. We also included selected literature results from both weak SOI (graphene,¹⁴⁻¹⁵ and GaN⁵⁷) and strong SOI materials (GaAs,^{12, 58} InAs,⁵⁹ and InSb⁶⁰).

Cite this: DOI: 10.1039/c0xx00000x

www.rsc.org/xxxxxx

REVIEW**Table 2.** Comparison of spin lifetime and diffusion length in semiconductor nanowires and bulk

SC		n or p (cm ⁻³)	FM	Barriers	Methods	T (K)	τ_{sf} (ns)	λ_{sf} (μ m)	Ref.
<i>n</i> -Si	NW	3×10^{19}	Co	Al ₂ O ₃	2-T/NL	5	90	6	[25]
	bulk	5×10^{19}	Fe	Al ₂ O ₃	NL	10	0.9	0.95	[51]
<i>n</i> -Ge	NW	9×10^{18}	Fe	MgO	NL	40	7.2	2.57	[20]
	bulk	2×10^{19}	Fe	MgO	NL	4	1.08	0.58	[10]
<i>p</i> -Ge	NW	8×10^{18}	Mn ₅ Ge ₃	Schottky	2-T	10	0.244	0.48	[19]
	bulk	8.2×10^{18}	Fe	MgO	3-T	5-300	0.013	0.08	[41]
<i>n</i> -GaN	NW	1×10^{17}	CoFe	MgO	NL	300	0.1	0.26	[23]
	bulk	4.2×10^{17}	MnAs	AlAs	3-T	300	0.044	0.175	[57]
<i>n</i> -InN	NW	1.1×10^{20}	Co	Al ₂ O ₃	NL	4	0.27	0.31	[24]

Elliott has shown that the electron spin relaxation time (spin lifetime) τ_{sf} is related to the elastic scattering time (momentum relaxation time) τ_e through the SOI in the case of Elliott-Yafet spin relaxation mechanism.⁶¹⁻⁶³

$$\frac{\tau_e}{\tau_{sf}} = \text{const} \propto \left(\frac{\lambda}{\Delta E}\right)^2 \quad (5),$$

where λ is the atomic SOI constant for a specific energy band, ΔE is the energy gap between the considered energy band and the nearest one that is coupled through the atomic SOI, and the ratio of τ_e/τ_{sf} is shown to be temperature independent. Although in compound materials (like GaAs) lacking crystal inversion symmetry, the D'yakonov-Perel' spin relaxation mechanism (mediated by intrinsic internal magnetic fields induced by inversion asymmetry) becomes important and even dominant,³ the general trend in **Fig. 4** qualitatively agrees with **Eq. (5)**: the stronger SOI strength, the stronger spin relaxation, and hence the smaller spin lifetime. It should be pointed out that SOI is not generally detrimental for spintronic device applications, because it also offers an important means for electrical spin manipulation (e.g., gate-controlled spin precession in Datta-Das spin-polarized FET, as to be discussed in Fig 10(a)).

3. Electrical spin transport in semiconductor nanostructures

3.1. Motivation from semiconductor bulk to nanostructures

To further explore new materials with long spin lifetime and diffusion length, low-dimensional semiconductor nanostructures have attracted considerable interest because of their unique physical properties for carrier and spin transport. For example, Ge/Si quantum well structures produce a high-mobility two-dimensional electron/hole gas channel, which may promise a long spin diffusion length. Ge/Si nanowires on the other hand provide a quasi-1-D channel with significant quantum confinements. In those low-dimensional Ge/Si nanostructures, the crystal inversion symmetry is not preserved (for example, the inversion symmetry in Ge/Si heterostructures is broken by the presence of asymmetric

confining potentials). Therefore, the absent D'yakonov-Perel' spin relaxation mechanism in bulk crystals may become appreciable in Ge/Si nanostructures. The breaking of inversion symmetry in quantum wells increases the SOI, which enhances the Rashba effect for gate modulation of the spin transport but meanwhile could decrease the spin lifetime. Although tremendous work has been done in the electrical spin injection into III-V based quantum wells,^{59, 64-66} little progress has been made yet on the electrical spin injection into Ge/Si quantum wells. Very recently, the optical spin injection into Ge/SiGe quantum wells was evidenced by the photoluminescence, showing a very short spin lifetime for holes of 0.5 ps.⁶⁷

Despite of the short spin lifetime in quantum well structures, semiconductor nanowires on the other hand could have very long spin lifetimes, even larger than those in bulk materials. This is because the phonon scattering is significantly suppressed in nanowires because of the reduced density of states,⁶⁸ so that the momentum relaxation and hence the spin relaxation is effectively reduced in the Elliott-Yafet mechanism. Also, the 1-D channel confines the momentum along the wire axis, and all the spin rotations are limited to a single axis; therefore, the spin dephasing induced by the randomizing momentum-dependent magnetic field in the D'yakonov-Perel' spin relaxation mechanism is minimized.²⁶ It has been experimentally observed that the spin relaxation rate in submicron InGaAs wires is significantly suppressed for widths up to one order of magnitude larger than the electron mean free path.⁶⁹⁻⁷⁰ Although surface roughness scattering, considering the large surface-to-volume ratio of nanowires, may contribute to additional spin relaxation,⁷¹ the suppressed Elliott-Yafet and D'yakonov-Perel' mechanisms, along with surface passivation and engineering, could effectively reduce the overall spin relaxation in nanowires compared with bulk materials. In fact, it has been experimentally demonstrated that spin relaxation can be suppressed by quantum confinements in both Ga_xIn_{1-x}As/InP quantum wires and InAs nanowires, as evidenced by the crossover from weak antilocalization effect to weak localization effect as the wire width (diameter) is reduced.⁷²⁻⁷⁴ Recently, there have been increasing efforts in realizing electrical spin injection into semiconductor nanowires

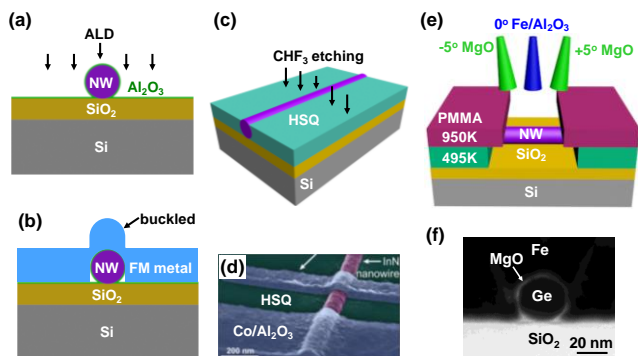


Fig. 5: Fabrication of ferromagnetic tunnel junctions on semiconductor nanowires. (a) Schematic illustration of the Al_2O_3 deposition on semiconductor nanowires by ALD as the tunneling oxide for spin injection. (b) Schematic illustration of the nanowire spin injection device after the ferromagnetic metal deposition, showing a buckled morphology on top of the nanowire. Reproduced with permission from Ref. [25]. Copyright 2013, American Chemical Society. (c) Schematic illustration of the planarization process using an HSQ lifting layer followed by CHF_3 plasma etching. (d) Colored SEM image of the fabricated nanowire spin injection device with smooth ferromagnetic contacts. Reproduced with permission from Ref. [24]. Copyright 2012, American Chemical Society. (e) Schematic illustration of the tilted three-step deposition process to grow $\text{Al}_2\text{O}_3/\text{Fe}/\text{MgO}$ tunnel junctions on Ge nanowires. (f) Cross-sectional TEM image of a $\text{Fe}/\text{MgO}/\text{Ge}$ nanowire tunnel junction, showing a uniform coverage of 2 nm MgO on the Ge nanowire surface. Reproduced with permission from ECS Trans., **64**, 613 (2014). Copyright 2014, The Electrochemical Society.

using both ferromagnetic tunneling and Schottky contacts. The observed spin lifetimes and diffusion lengths in nanowires, including Ge,¹⁹⁻²¹ Si,^{22, 25} GaN,²³ and InN,²⁴ are indeed much larger than those reported in their bulk counterparts. **Table 2** summarizes the results from literature for comparison, and the experimental details will be reviewed as follows.

3.2. Tunneling contact spin injection into semiconductor nanowires

Experimentally, the cylindrical geometry of nanowires has been a major challenge in depositing high-quality tunnel oxides or Schottky contacts on nanowire surface for spin injection. Firstly, there is no well-defined lattice plane on the curved nanowire surface; therefore, the favorable epitaxial growth of tunnel oxide (*i.e.*, $[110]\text{Fe}(001) // [100]\text{MgO}(001) // [110]\text{Ge}(001)$ in the $\text{Fe}/\text{MgO}/\text{Ge}$ epitaxial tunnel junction³⁰) can hardly be utilized in nanowire devices. Secondly, the high surface-to-volume ratio of nanowires yields a large surface area with a high density of interface states, as usually evidenced by the large gate hysteresis in nanowire transistors.⁴⁶ Such a high density of interface states would lead to strong Fermi-level pinning in ferromagnetic metal contacts, which could jeopardize the spin injection process.

In the efforts of fabricating high-quality ferromagnetic tunneling contacts to semiconductor nanowires, several approaches have been employed, as illustrated in **Fig. 5**. Firstly, atomic-layer deposition (ALD) was used to grow conformal Al_2O_3 tunnel oxide on Si nanowires as shown in **Fig. 5(a)**,²⁵ however, the nucleation of ALD is very sensitive to the initial surface condition and the ALD films may be discontinuous with pinholes in the ultrathin film regime.⁷⁵ Besides, the metal electrode, which is usually deposited by directional electron beam evaporation, is buckled on top of the nanowire as schematically illustrated in **Fig. 5(b)**. Such contact morphology would prevent abrupt switchings of the magnetization,²⁵ especially for nanowires with large diameters (which essentially require thick

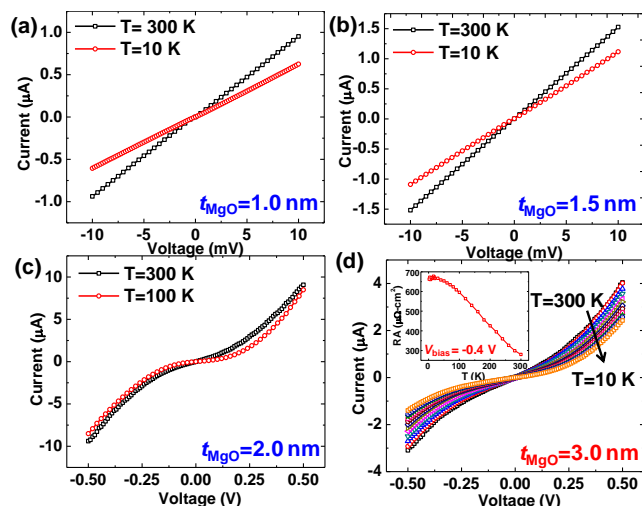


Fig. 6: Ferromagnetic Fe/MgO tunnel junctions on Ge nanowires. Temperature-dependent I - V curves of a series of $\text{Fe}/\text{MgO}/\text{Ge}$ nanowire devices with nominal MgO thickness of (a) 1.0 nm, (b) 1.5 nm, (c) 2.0 nm, and (d) 3.0 nm, respectively. For MgO thickness of 1.0 nm and 1.5 nm, the I - V curves are linear, implying pinholes may exist in the ultrathin MgO films on the Ge nanowire surface. However, as the MgO thickness reaches 2.0 nm and 3.0 nm, the I - V curves become nonlinear, suggesting apparent tunneling behaviors for slightly thicker MgO. The inset of (d) shows the RA product extracted from the temperature-dependent I - V curves at a bias voltage of 0.4 V for the MgO thickness of 3.0 nm. The weak temperature dependence affirms the tunneling nature for the $\text{Fe}/\text{MgO}/\text{Ge}$ nanowire junction. Reproduced with permission from ECS Trans., **64**, 613 (2014). Copyright 2014, The Electrochemical Society.

metal electrodes). To solve this issue, Heedt *et al* proposed a planarization procedure using a hydrogen silsesquioxane (HSQ) lifting layer to reduce the metal electrode thickness and hence make smooth ferromagnetic contacts to cylindrical nanowires,²⁴ as shown in **Fig. 5(c-d)**. This process is useful for nanowires with facets and large diameters; however, it is susceptible to the nonuniformity of the nanowire diameters and also process variations (such as the HSQ thickness and etching depth). Alternatively, a tilted three-step deposition process has been used to grow high-quality Fe/MgO tunnel junctions on Ge nanowires inside an MBE chamber, as illustrated in **Fig. 5(e)**. Firstly 0.5- t -thick MgO was deposited under +5 degree tilting and then 0.5- t -thick MgO deposition under -5 degree tilting (t is the nominal total thickness of the MgO tunnel oxide). Finally 120 nm-thick Fe was deposited with normal incidence (0 degree tilting) followed by 10 nm-thick Al_2O_3 capping to prevent Fe oxidation. The purpose of this tilted deposition process is to promote a good coverage of MgO on the nanowire surface and hence minimize undesirable short circuit between the Fe electrode and Ge nanowire. Indeed, cross-sectional TEM image of the grown $\text{Fe}/\text{MgO}/\text{Ge}$ nanowire tunnel junction revealed a relatively uniform coverage of MgO on the Ge nanowire surface, as shown in **Fig. 5(f)**.

To obtain an electrically functional tunnel junction on n -Ge nanowires for spin injection, the tunnel oxide MgO thickness was fine tuned. **Fig. 6** shows the temperature-dependent I - V characteristics of $\text{Fe}/\text{MgO}/\text{Ge}$ nanowire devices with nominal MgO thickness from 1 nm to 3 nm.²⁰ We can see that for MgO nominal thickness of 1.0 nm and 1.5 nm, the I - V curves were linear from 300 K to 10 K, implying that there might be pinholes or leakage paths in the ultrathin MgO oxide layer. However, as the MgO nominal thickness is increased to 2.0 nm and 3.0 nm, the current decreased dramatically, and more importantly the I - V curves became nonlinear, suggesting apparent

Cite this: DOI: 10.1039/c0xx00000x

www.rsc.org/xxxxxx

REVIEW

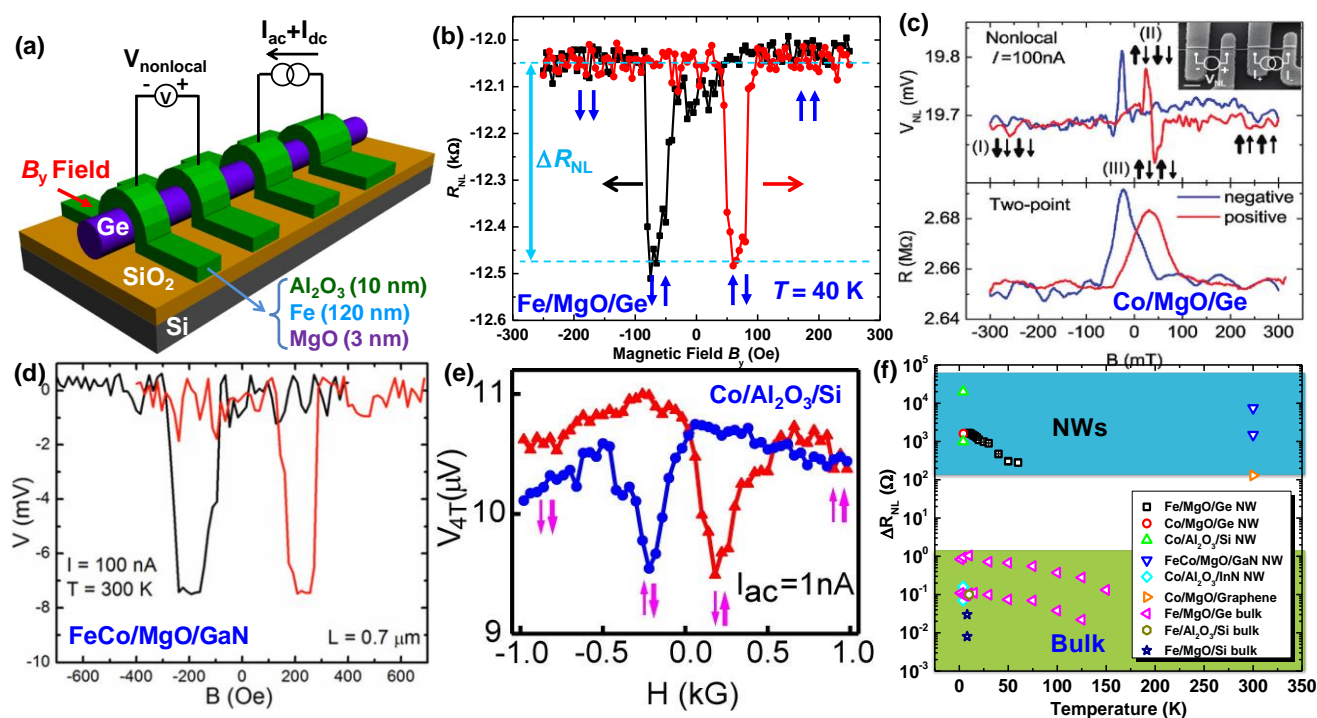


Fig. 7: Tunneling contact spin injection into semiconductor nanowires. (a) Schematic illustration of the nonlocal spin valve measurement setup for Ge nanowires with Fe/MgO tunnel junctions. (b) Nonlocal spin valve signal of *n*-type Ge nanowires at $T = 40$ K with an injection ac current of $1 \mu\text{A}$, showing a nonlocal resistance change of $\Delta R_{NL} = 470 \Omega$. The black and red arrows indicate the sweeping direction of the magnetic field, while the blue arrows denote the relative magnetization direction of the spin injector and detector, respectively. (c-e) Nonlocal spin valve signals observed in Ge, GaN, and Si nanowires, and bulk materials. (f) Comparison of temperature-dependent nonlocal resistance change reported in various semiconductor nanowires and bulk as well as graphene. The observed nonlocal resistance change in nanowire devices is typically orders of magnitudes larger than that in bulk devices (only exception is the InN nanowire). (a-b) and (f) are reproduced with permission from ECS Trans., **64**, 613 (2014). Copyright 2014, The Electrochemical Society. (c) is reproduced with permission from Ref. [21]. Copyright 2010, American Chemical Society. (d) is reproduced with permission from Ref. [23]. Copyright 2012, AIP Publishing LLC. (e) is reproduced with permission from Ref. [25]. Copyright 2013, American Chemical Society.

tunneling behaviors for slightly thicker MgO. It should be pointed out that the critical MgO thickness in Ge nanowire devices (about 2 nm) to achieve tunneling behavior is larger than the value in thin film devices (about 0.5-1 nm).^{10, 38} This is because the Ge thin film has a much flatter surface morphology that allows for a smooth coverage of MgO on the Ge surface during the deposition process. Nevertheless, the weak temperature dependence of the resistance-area (RA) product shown in the inset of Fig. 6(d) affirms the tunneling nature of the Fe/MgO/Ge nanowire junction. Similarly, the three measurement techniques for bulk/thin films discussed previously can also be used to study the spin transport in semiconductor nanowires: 3-T Hanle, nonlocal (4-T) Hanle, and nonlocal spin valve measurements. In practice, however, considering the small diameter of nanowires, the contact area in nanowire spin injection devices is typically much smaller than that of bulk devices, and hence the 3-T Hanle signal would be too small to detect. Also, the spin precession in an ideally 1-D channel is expected to be confined to the nanowire axis, which could make the nonlocal Hanle signal difficult to be observed. In fact, to the best of our knowledge, the only report of nonlocal Hanle signal was in GaN nanowires with FeCo/MgO tunnel contacts.²³ Meanwhile, nonlocal spin valve signals have been observed in several other semiconductor nanowires, including Ge,²⁰⁻²¹ Si,²⁵ and InN,²⁴ which are usually considered as

a clear evidence for successful spin injection. Similar to spin injection in bulk, the nonlocal spin valve measurement setup is shown in Fig. 7(a) for spin injection into *p*-Ge nanowires with MBE-grown Fe/MgO tunnel junctions, and Fig. 7(b) shows the nonlocal spin valve signal in *n*-type Ge nanowires at $T = 40$ K. Using Eq. (2), the spin diffusion length can be extracted as $\lambda_{sf} = 2.57 \mu\text{m}$ in the *n*-Ge nanowire, and the spin lifetime can be further calculated to be $\tau_{sf} = 7.2$ ns. Both values are larger than those reported in bulk *n*-Ge ($\lambda_{sf} = 0.58 \mu\text{m}$ and $\tau_{sf} = 1.08$ ns) with a similar doping level ($N_D \approx 10^{19} \text{cm}^{-3}$).¹⁰ Similarly, Figs. 7(c-e) depict the literature-reported nonlocal spin valve measurements for Ge,²¹ Si,²⁵ and InN nanowires,²⁴ respectively. For comparison, the change of the observed nonlocal spin valve signal, namely the nonlocal resistance ΔR_{NL} , in nanowire devices is much larger than the values observed in the bulk devices (one exception is the InN nanowire, possibly due to a rather small contact resistance and P_1 , or a relatively large σ_s), as summarized in Fig. 7(f). This is mainly because that the channel cross-sectional area in nanowire devices is much smaller, which would give rise to a larger nonlocal spin valve signal according to Eq. (2). Besides, longer spin diffusion length in nanowires compared with bulk materials would enhance the nonlocal spin valve signal as well. Admittedly, there may be small variations in σ_s and P_1

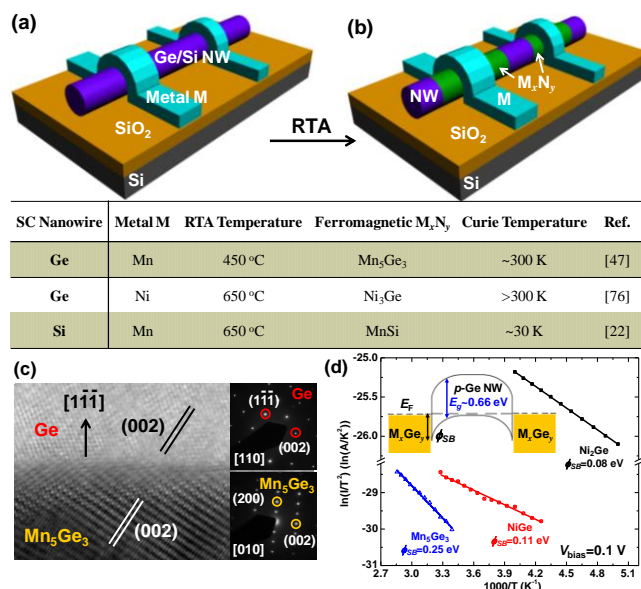


Fig. 8: Fabrication of ferromagnetic Schottky contacts in semiconductor nanowires. (a-b) Schematic illustration of the formation of Ge/Si nanowire transistors *via* RTA. The formed single-crystalline germanide/silicide regions with atomically smooth interfaces are used as high-quality Schottky source/drain contacts. The table below summarizes the formation of several ferromagnetic germanides and silicide for spintronic applications. (c) High-resolution TEM image of the formed Mn_5Ge_3/Ge nanowire heterostructure, showing an atomically smooth interface and high-quality epitaxial relationship. The insets are the diffraction patterns for Ge and Mn_5Ge_3 , respectively. Reproduced with permission from Ref. [47]. Copyright 2012, American Chemical Society. (d) Arrhenius plots for three Ge nanowire transistors at a bias voltage of 0.1 V. The extracted Schottky barrier heights for the Ni_2Ge , NiGe and Mn_5Ge_3 in contact with *p*-Ge are 0.08 eV, 0.11 eV and 0.25 eV, respectively. The inset shows the energy band diagram for the $M_xGe_y/Ge/M_xGe_y$ nanowire transistor. The change in the Schottky barrier height with different germanide contacts suggests that Fermi level pinning is alleviated with these high-quality germanide contacts. © 2012 IEEE. Reproduced, with permission, from Ref. [78]: 2012 12th IEEE Conference on Nanotechnology (IEEE-NANO).

for different materials that can also affect the observed ΔR_{NL} . Fig. 7(f) intends to show a general trend of larger ΔR_{NL} in semiconductor nanowires, which could be advantageous for spin signal sensing at a given injection current. A direct comparison of the spin diffusion length (λ_{sf}) and spin lifetime (τ_{sf}) between semiconductor nanowires and bulk is made in Table 2. These results imply that reduced dimensionality indeed helps suppress the spin relaxation in semiconductors.

3.3. Schottky contact spin injection into semiconductor nanowires

Besides to the above-discussed tunneling barriers on semiconductor nanowires for spin injection, Schottky barriers are another approach to circumvent the conductivity mismatch problem in realizing appreciable spin injection efficiency into nanowires.²⁸ However, because of the cylindrical geometry of semiconductor nanowires, the epitaxial growth of high-quality ferromagnetic Schottky contacts on nanowires is very difficult. Alternatively, a convenient contact engineering method using RTA has been established to fabricate high-quality silicide/germanide Schottky contacts in Si/Ge nanowires with atomically clean interfaces,⁷⁶⁻⁷⁷ as illustrated in **Figs. 8(a-b)** (see recent review articles Ref. [76] and Ref. [77]). This unique 1-D growth mode has many merits in fabricating high-performance electronic and spintronic devices. Firstly, the formed

silicide/germanide contacts are typically single-crystalline,^{22, 44-47} and always maintain atomically clean interfaces with the Ge/Si nanowires (see **Figs. 2(c)** and **8(c)**), even in the presence of a large lattice mismatch at the interface or a huge strain in the nanowire heterostructure. Unlike conventional thin film epitaxy, this unique growth mode in the 1-D regime is able to sustain substantially large lattice mismatch because of quantum confinements.⁴⁷ Besides, the atomically clean interface helps alleviate the Fermi level pinning in conventional metal/semiconductor direct contacts, and hence facilitates the electron and spin transport. This is evidenced by the change of Schottky barrier height in Ge nanowires with different germanide contacts formed by RTA, as shown in **Fig. 8(d)**, which is clearly different from the scenario in **Fig. 1(a)** with strong Fermi level pinning.⁷⁸ Moreover, the Si/Ge nanowire channel length can be easily scaled down to sub-tens nm by controlling the annealing time and temperature.^{22, 47, 76} This approach hence provides a simple and low-cost method to fabricate nanowire transistors with a precisely controlled nanoscale channel length using a facile RTA process.

Recently, the above approach has been used to form single-crystalline ferromagnetic Schottky contacts in Si/Ge nanowires with atomically clean interfaces for spin transport studies.^{19, 22, 47} In general, the Curie temperature of ferromagnetic germanides is much higher than that of ferromagnetic silicides, which offers an important advantage for Ge-based materials over Si-based materials for high-temperature spintronic devices. Unfortunately, standard nonlocal spin valve measurement cannot be performed in such Ge/Si nanowire heterostructure devices, because the ferromagnetic germanide/silicide contacts are formed inside rather than on top of the Ge/Si nanowire channel and hence the channel is not continuous but isolated into segments by the ferromagnetic contacts.¹⁹ Alternatively, the formed Ge/Si nanowire heterostructure can be treated as a vertical spin valve with a current perpendicular-to-plane configuration.⁷⁹⁻⁸⁰ Take the Mn_5Ge_3/p -Ge/ Mn_5Ge_3 nanowire transistor as an example shown in **Fig. 9(a)**. In this case, under a finite source-drain bias, spin-polarized carriers are injected into the Ge nanowire from one ferromagnetic Mn_5Ge_3 contact (namely the spin injector) through a Schottky barrier, and are then scattered as they travel along the Ge nanowire channel before reaching the other ferromagnetic Mn_5Ge_3 contact (namely the spin detector). This process is schematically illustrated in **Fig. 9(b)**. The easy-axis of the ferromagnetic Mn_5Ge_3 contact is found to be along the nanowire axis because of the shape anisotropy.⁸¹ For the spin injection measurement, an axial magnetic field was swept back and forth to change the relative magnetization directions of the spin injector and detector between parallel and anti-parallel states, representing low and high resistance states, respectively. **Fig. 9(c)** shows the MR curves of three $Mn_5Ge_3/Ge/Mn_5Ge_3$ nanowire transistors with different channel lengths ($L_{ch} = 450, 550, \text{ and } 700 \text{ nm}$) at $T = 10 \text{ K}$ under a dc current bias of $I_{dc} = 10 \mu\text{A}$.¹⁹ The negative and hysteretic MR characteristics indicated successful spin injection in the Ge nanowire transistor. Likewise, similar MR behavior was also observed in the $MnSi/Si/MnSi$ nanowire heterostructure, in which the ferromagnetic Schottky $MnSi$ contacts served as the spin injector and detector, as shown in **Figs. 9(d-e)**.²² It is noted that the observed MR characteristics do not resemble typical spin valve signal with abrupt resistance steps, which correspond to the magnetization switching of the spin injector and detector successively.⁷⁹⁻⁸⁰ This is likely due to the presence of multiple domains in the formed ferromagnetic contacts and small difference in their coercive fields,⁸¹ which is limited by the device structure and the fabrication process itself.

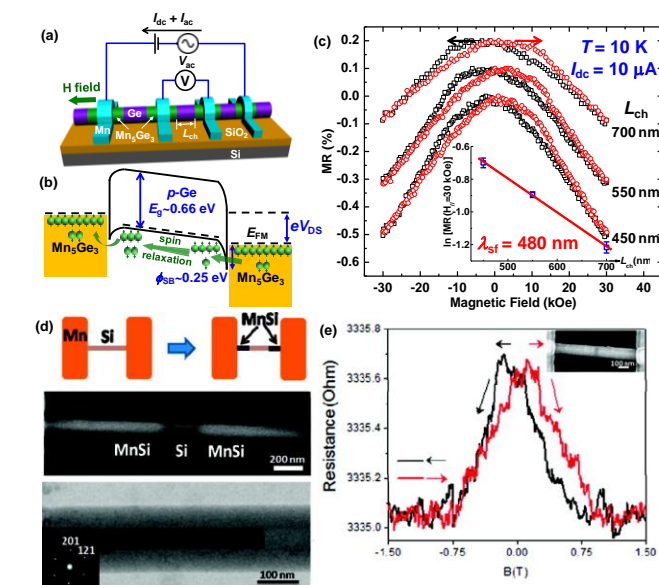


Fig. 9: Schottky contact spin injection into semiconductor nanowires. (a) Schematic illustration of a $\text{Mn}_5\text{Ge}_3/\text{Ge}/\text{Mn}_5\text{Ge}_3$ nanowire device with spin injection measurement setup. (b) Energy band diagram of the p -type $\text{Mn}_5\text{Ge}_3/\text{Ge}/\text{Mn}_5\text{Ge}_3$ nanowire transistor to schematically illustrate the transport process of spin-polarized carriers. (c) MR curves of three $\text{Mn}_5\text{Ge}_3/\text{Ge}/\text{Mn}_5\text{Ge}_3$ nanowire transistor with different channel lengths ($L_{\text{ch}} = 450, 550, \text{ and } 700 \text{ nm}$) at $T = 10 \text{ K}$ under a dc current bias of $I_{\text{dc}} = 10 \mu\text{A}$. The black and red arrows indicate the backward and forward sweeping directions of the axial magnetic field, respectively. All the MR curves are intentionally offset by multiples of 0.1% for clarity. The inset shows the semi-log plot of the MR magnitude at $H_{\parallel} = 30 \text{ kOe}$ versus the channel length, in which the linear fitting (red curve) yields a spin diffusion length of $\lambda_{\text{sf}} = 480 \pm 13 \text{ nm}$ in the p -Ge nanowire at $T = 10 \text{ K}$. (d) TEM images of the formation of $\text{MnSi}/\text{Si}/\text{MnSi}$ nanowire heterostructure. (e) The resistance change of the $\text{MnSi}/p\text{-Si}/\text{MnSi}$ nanowire heterostructure as a function of magnetic field, showing a hysteretic behavior. The inset shows the device SEM image.

The spin diffusion length can be extracted from the channel length-dependent MR signals using the modified Julliere's model to take into account the spin relaxation in the nanowire channel:⁸²

$$\text{TMR} = \frac{2P_1P_2e^{-\frac{L_{\text{ch}}}{\lambda_{\text{sf}}}}}{1 + P_1P_2e^{-\frac{L_{\text{ch}}}{\lambda_{\text{sf}}}}} \quad (6),$$

where P_1 and P_2 are the spin polarizations of the two FM electrodes, L_{ch} is the Ge nanowire channel length, and λ_{sf} is again the spin diffusion length. Based on this model, the spin diffusion length in the p -type Ge nanowire at $T = 10 \text{ K}$ was extracted to be $\lambda_{\text{sf}} = 480 \pm 13 \text{ nm}$, as shown in the inset of **Fig. 9(c)**, and the spin lifetime was further calculated to be about $\tau_{\text{sf}} = 244 \text{ ps}$.¹⁹ Notably, both values in the p -type Ge nanowire exhibited more than one order of magnitude enhancement over those reported for bulk p -type Ge with a similar doping level ($N_A \approx 8 \times 10^{18} \text{ cm}^{-3}$). Again, this result affirms that the spin relaxation is indeed suppressed in nanowires compared with semiconductor bulk.

Conclusions and perspective

In sum, tremendous efforts have been devoted to the study of electrical spin injection and transport in various semiconductors.

Earlier work has been mainly focused on bulk semiconductors and thin films, given that they are easy to tune the doping profile and fabricate into devices. Semiconductor nanostructures, in particular nanowires, are usually challenging to fabricate high-quality ferromagnetic contacts for spin transports studies because of their curved geometry. Recent efforts have been made to demonstrate electrical spin injection in several semiconductor nanowires (including Si, Ge, GaN, and InN) using both ferromagnetic tunnel junctions and Schottky contacts. Inspiringly, the observed spin lifetime and spin diffusion length in semiconductor nanowires are much higher than those reported in bulk/thin film counterparts. As a signature for successful spin injection, the nonlocal spin valve signals in nanowire spin injection devices are typically orders of magnitudes higher than those observed in bulk devices. These results suggest that the spin relaxation is indeed suppressed in semiconductor nanowires, and it implies the advantage of using low-dimensional semiconductor nanostructures in making practical spintronic devices with long spin lifetime and spin diffusion length.

In the future, more and more research efforts are expected to devote to the realization of spin injection into different semiconductor nanowires (as well as nanoribbons). By playing with different parameters in nanowire spin injection devices, it would be of fundamental interest and significance to investigate the diameter effect (size-induced quantum confinements), the doping effect (impurity-induced spin relaxation) and the surface effect (interface states and surface roughness scattering) on the underlying spin transport. Besides, many core/shell nanowires with a 1-D hole/electron gas, such as Ge/Si and GaAs/AlGaAs core/shell nanowires,⁸³⁻⁸⁵ could provide another degree of freedom to tune the nanowire structure and hence the spin transport properties for building practical spintronic devices. Furthermore, it would be interesting to investigate the effect of SOI on the spin relaxation and the observed spin lifetime. The literature review on bulk materials in this paper already indicates a general trend that strong SOI degrades the spin lifetime. On the other hand, the recently discovered topological insulators with extremely strong SOI exhibit unique spin-polarized surface states with inherent spin-momentum locking,⁸⁶ which provides another interesting platform to study the spin transport in the presence of strong SOI.

It should be noticed that research of semiconductor spintronics so far has been mainly focused on studies of the charge-spin transport and spin dynamics. Through extensive spin transport measurements, the observed spin diffusion length in many materials (typically hundreds of nanometers) is already much larger than the channel length of state-of-the-art MOS transistors. The advanced microelectronics technology has provided us with many sophisticated and reliable fabrication techniques. Therefore, the future of spintronics should involve more efforts in building practical spintronic devices that can provide nonvolatility, low energy dissipation, high switching speed, and many other advantages over conventional Si CMOS devices. In fact, several prototypes of spinFETs have been proposed as shown in **Fig. 10**, and in the meanwhile, theoretical modeling and experimental implementations have also been attempted. For example, as shown in **Fig. 10(a)**, Datta and Das proposed a spin-polarized FET as an electronic analog to the electro-optic modulator,¹⁷ in which spin-polarized electrons are injected into a semiconductor channel from one ferromagnetic contact (spin injector or polarizer), then the electron spin precession is modulated by the gate voltage through the Rashba effect,⁸⁷ and is finally probed by the other ferromagnetic contact (spin detector or analyzer). Here the gate-modulated spin precession relies on the strength of SOI in the channel; therefore, there is a tradeoff between the spin

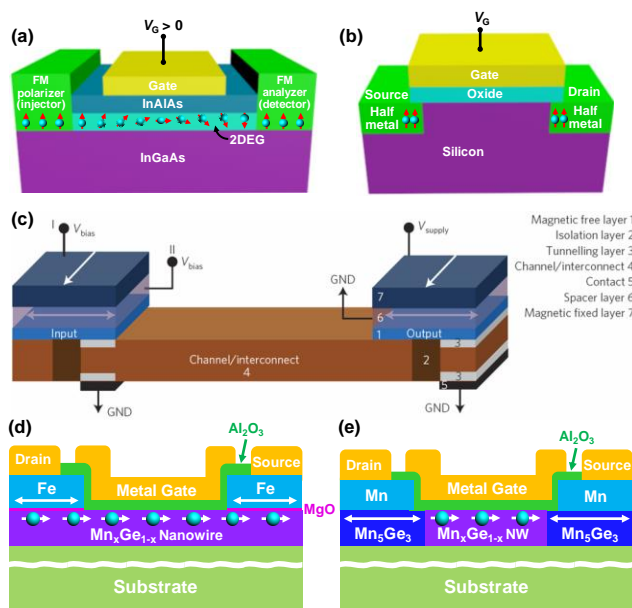


Fig. 10: Schematic illustrations of various proposals of spinFETs. (a) Datta-Das type spin-polarized FET with gate-modulated spin precession through the Rashba effect. Reproduced with permission from Ref. [17]. Copyright 1990, AIP Publishing LLC. (b) Sugahara-Tanaka type spin-MOSFET with half-metallic source/drain contacts. Reproduced with permission from Ref. [18]. Copyright 2004, AIP Publishing LLC. (c) all-spin logic device with input and output nanomagnets (built-in memory) that communicate through the spin-coherent channel. Reproduced by permission from Macmillan Publishers Ltd: Nature Nanotechnology, **5**, 266 (2010), copyright 2010. (d-e) diluted magnetic Ge nanowire-based nonvolatile transpinor with Fe/MgO tunnel junctions and ferromagnetic Mn_5Ge_3 Schottky junctions, respectively. Reproduced with permission from ECS Trans., **64**, 613 (2014). Copyright 2014, The Electrochemical Society.

diffusion length and the Rashba effect strength when choosing the appropriate channel material for the device implementation. Another variant using single-spin manipulation plus metallic ferromagnets, proposed by Sugahara and Tanaka,¹⁸ is a spin-MOSFET comprised of an ordinary MOSFET with half-metallic source/drain contacts, in which the gate electrode modulates the Schottky barrier shape at the source/drain junctions and hence the current, as shown in Fig. 10(b). Besides, Behin-Aein *et al* proposed an interesting all-spin logic device with built-in memory that uses spin at every stage of its operation to avoid repeated spin-to-charge conversion, which could help reduce the power dissipation.⁸⁸ The device structure is schematically shown in Fig. 10(c), in which the input and output information are stored as the magnetization of nanomagnets that communicate through a spin-coherent semiconductor or metal channel. More recently, to minimize the energy-dissipative charge current flow, a novel transpinor has been proposed with diluted magnetic semiconductor (DMS), whose ferromagnetism can be controlled by an external electric field.⁸⁹ Two prototypes are shown in Figs. 10(d-e), in which ferromagnetic Fe/MgO tunnel junctions and Mn_5Ge_3 Schottky contacts are integrated on a $\text{Mn}_x\text{Ge}_{1-x}$ DMS nanowire channel for spin injection and detection, respectively. Unlike the Datta-Das spin-polarized FET relying on the Rashba effect to control the spin precession of individual electrons, the proposed transpinor rather manipulates a collection of spins as a single entity *via* the carrier-mediated magnetic phase transition and thus is more energy-efficient and robust.⁹⁰

Admittedly, each proposed device concept has its own merits and challenges to be solved. It should be pointed out that one of

the key challenges to integrate spintronic devices into CMOS circuits is to achieve efficient conversion between a spin signal (magnetization) and a charge signal (current/voltage), and the concatenability (device fan out). Novel device concepts and materials may be required to realize spin-based information processing while minimizing dissipative charge current flow. In the implementation of practical spintronic devices, low-dimensional nanostructures, especially Ge/Si nanowires, could be a promising material candidate because of their long spin lifetime and diffusion length as well as their easy integration with mainstream Si technology.

Acknowledgment

The authors would like to acknowledge the support from National Science Foundation under grant ECCS 1308358. This work was also supported by Western Institution of Nanoelectronics (WIN). The authors also acknowledge Chiu-Yen Wang, Lih-Juann Chen, Patrick M. Odenthal, Wei Han, Roland Kawakami, Li-Te Chang, Yi Zhou for help in device fabrication and measurements. K. L. Wang acknowledges the support of the Raytheon endowment for the Chair Professorship.

Notes and references

- ^a Device Research Laboratory, Department of Electrical Engineering, University of California, Los Angeles, California, 90095, USA. Tel: 310-825-1609; E-mail: tjianshi@ucla.edu, wang@ee.ucla.edu
- ^b Present address: IBM Thomas J. Watson Research Center, Yorktown Heights, NY 10598, USA; Tel: 914-945-1524; E-mail: jwang@us.ibm.com
1. International Technology Roadmap of Semiconductors (ITRS), <http://www.itrs.net>, 2013 Edition.
2. S. A. Wolf, D. D. Awschalom, R. A. Buhrman, J. M. Daughton, S. v. Molnar, M. L. Roukes, A. Y. Chtchelkanova and D. M. Treger, *Science*, 2001, 294, 1488-1495.
3. I. Žutić, J. Fabian and S. Das Sarma, *Rev. Mod. Phys.*, 2004, 76, 323-410.
4. M. N. Baibich, J. M. Broto, A. Fert, F. N. Van Dau, F. Petroff, P. Etienne, G. Creuzet, A. Friederich and J. Chazelas, *Phys. Rev. Lett.*, 1988, 61, 2472.
5. G. Binasch, P. Grünberg, F. Saurenbach and W. Zinn, *Phys. Rev. B*, 1989, 39, 4828.
6. F. J. Jedema, A. T. Filip and B. J. van Wees, *Nature*, 2001, 410, 345-348.
7. F. J. Jedema, H. B. Heersche, A. T. Filip, J. J. A. Baselmans and B. J. van Wees, *Nature*, 2002, 416, 713-716.
8. B. T. Jonker, G. Kioseoglou, A. T. Hanbicki, C. H. Li and P. E. Thompson, *Nature Phys.*, 2007, 3, 542-546.
9. S. P. Dash, S. Sharma, R. S. Patel, M. P. de Jong and R. Jansen, *Nature*, 2009, 462, 491-494.
10. Y. Zhou, W. Han, L.-T. Chang, F. Xiu, M. Wang, M. Oehme, I. A. Fischer, J. Schulze, R. K. Kawakami and K. L. Wang, *Phys. Rev. B*, 2011, 84, 125323.
11. K.-R. Jeon, B.-C. Min, Y.-H. Jo, H.-S. Lee, I.-J. Shin, C.-Y. Park, S.-Y. Park and S.-C. Shin, *Phys. Rev. B*, 2011, 84, 165315.
12. X. Lou, C. Adelman, S. A. Crooker, E. S. Garlid, J. Zhang, K. S. M. Reddy, S. D. Flexner, C. J. Palmstrom and P. A. Crowell, *Nature Phys.*, 2007, 3, 197-202.
13. H. J. Zhu, M. Ramsteiner, H. Kostial, M. Wassermeier, H.-P. Schönherr and K. H. Ploog, *Phys. Rev. Lett.*, 2001, 87, 016601.
14. N. Tombros, C. Jozsa, M. Popinciuc, H. T. Jonkman and B. J. van Wees, *Nature*, 2007, 448, 571-574.
15. W. Han, K. Pi, K. M. McCreary, Y. Li, J. J. I. Wong, A. G. Swartz and R. K. Kawakami, *Phys. Rev. Lett.*, 2010, 105, 167202.
16. M. Johnson, *Science*, 1993, 260, 320-323.
17. S. Datta and B. Das, *Appl. Phys. Lett.*, 1990, 56, 665-667.
18. S. Sugahara and M. Tanaka, *Appl. Phys. Lett.*, 2004, 84, 2307-2309.

19. J. Tang, C.-Y. Wang, L.-T. Chang, Y. Fan, T. Nie, M. Chan, W. Jiang, Y.-T. Chen, H.-J. Yang, H.-Y. Tuan, L.-J. Chen and K. L. Wang, *Nano Lett.*, 2013, 13, 4036-4043.
20. J. Tang, T. Nie and K. L. Wang, *ECS Trans.*, 2014, 64, 613-623.
21. E.-S. Liu, J. Nah, K. M. Varahramyan and E. Tutuc, *Nano Lett.*, 2010, 10, 3297-3301.
22. Y.-C. Lin, Y. Chen, A. Shailos and Y. Huang, *Nano Lett.*, 2010, 10, 2281-2287.
23. H. Kum, J. Heo, S. Jahangir, A. Banerjee, W. Guo and P. Bhattacharya, *Appl. Phys. Lett.*, 2012, 100, 182407.
24. S. Heedt, C. Morgan, K. Weis, D. E. Bürgler, R. Calarco, H. Hardtdegen, D. Grützmacher and Th. Schäfers, *Nano Lett.*, 2012, 12, 4437-4443.
25. S. Zhang, S. A. Dayeh, Y. Li, S. A. Crooker, D. L. Smith and S. T. Picraux, *Nano Lett.*, 2013, 13, 430-435.
26. A. A. Kiselev and K. W. Kim, *Phys. Rev. B*, 2000, 61, 13115-13120.
27. G. Schmidt, D. Ferrand, L. W. Molenkamp, A. T. Filip and B. J. van Wees, *Phys. Rev. B*, 2000, 62, R4790-R4793.
28. A. Fert and H. Jaffrès, *Phys. Rev. B*, 2001, 64, 184420.
29. E. I. Rashba, *Phys. Rev. B*, 2000, 62, R16267-R16270.
30. W. Han, Y. Zhou, Y. Wang, Y. Li, J. J. I. Wong, K. Pi, A. G. Swartz, K. M. McCreary, F. Xiu, K. L. Wang, J. Zou and R. K. Kawakami, *J. Cryst. Growth*, 2009, 312, 44-47.
31. K. Yamane, K. Hamaya, Y. Ando, Y. Enomoto, K. Yamamoto, T. Sadoh and M. Miyao, *Appl. Phys. Lett.*, 2010, 96, 162104.
32. S. P. Dash, S. Sharma, J. C. Le Breton, J. Peiro, H. Jaffrès, J. M. George, A. Lemaître and R. Jansen, *Phys. Rev. B*, 2011, 84, 054410.
33. A. Toriumi, T. Tabata, C. Hyun Lee, T. Nishimura, K. Kita and K. Nagashio, *Microelectron. Eng.*, 2009, 86, 1571-1576.
34. V. Heine, *Phys. Rev.*, 1965, 138, A1689-A1696.
35. R. R. Lieten, S. Degroote, M. Kuijk and G. Borghs, *Appl. Phys. Lett.*, 2008, 92, 022106.
36. T. Nishimura, K. Kita and A. Toriumi, *Appl. Phys. Express*, 2008, 1, 051406.
37. Y. Zhou, M. Ogawa, X. Han and K. L. Wang, *Appl. Phys. Lett.*, 2008, 93, 202105.
38. Y. Zhou, W. Han, Y. Wang, F. Xiu, J. Zou, R. K. Kawakami and K. L. Wang, *Appl. Phys. Lett.*, 2010, 96, 102103.
39. W. H. Butler, X. G. Zhang, T. C. Schulthess and J. M. MacLaren, *Phys. Rev. B*, 2001, 63, 054416.
40. T. Sasaki, T. Oikawa, T. Suzuki, M. Shiraishi, Y. Suzuki and K. Noguchi, *Appl. Phys. Lett.*, 2010, 96, 122101.
41. S. Iba, H. Saito, A. Spiesser, S. Watanabe, R. Jansen, S. Yuasa and K. Ando, *Appl. Phys. Express*, 2012, 5, 053004.
42. Y. Zhou, M. Ogawa, M. Bao, W. Han, R. K. Kawakami and K. L. Wang, *Appl. Phys. Lett.*, 2009, 94, 242104.
43. K. Kasahara, Y. Baba, K. Yamane, Y. Ando, S. Yamada, Y. Hoshi, K. Sawano, M. Miyao and K. Hamaya, *J. Appl. Phys.*, 2012, 111, 07C503.
44. Y. Wu, J. Xiang, C. Yang, W. Lu and C. M. Lieber, *Nature*, 2004, 430, 61-65.
45. J. Tang, C.-Y. Wang, F. Xiu, A. J. Hong, S. Chen, M. Wang, C. Zeng, H.-J. Yang, H.-Y. Tuan, C.-J. Tsai, L. J. Chen and K. L. Wang, *Nanotechnology*, 2010, 21, 505704.
46. J. Tang, C.-Y. Wang, F. Xiu, M. Lang, L.-W. Chu, C.-J. Tsai, Y.-L. Chueh, L.-J. Chen and K. L. Wang, *ACS Nano*, 2011, 5, 6008-6015.
47. J. Tang, C.-Y. Wang, M.-H. Hung, X. Jiang, L.-T. Chang, L. He, P.-H. Liu, H.-J. Yang, H.-Y. Tuan, L.-J. Chen and K. L. Wang, *ACS Nano*, 2012, 6, 5710-5717.
48. R. Jansen, S. P. Dash, S. Sharma and B. C. Min, *Semicond. Sci. Technol.*, 2012, 27, 083001.
49. L.-T. Chang, W. Han, Y. Zhou, J. Tang, I. A. Fischer, M. Oehme, J. Schulze, R. K. Kawakami and K. L. Wang, *Semicond. Sci. Technol.*, 2013, 28, 015018.
50. I. Appelbaum, B. Huang and D. J. Monsma, *Nature*, 2007, 447, 295-298.
51. O. van 't Erve, C. Awo-Affouda, A. T. Hanbicki, C. H. Li, P. E. Thompson and B. T. Jonker, *IEEE Trans. Electron Devices*, 2009, 56, 2343-2347.
52. T. Sasaki, T. Oikawa, M. Shiraishi, Y. Suzuki and K. Noguchi, *Appl. Phys. Lett.*, 2011, 98, 012508-012503.
53. C. H. Li, O. M. J. van 't Erve and B. T. Jonker, *Nature Commun.*, 2011, 2, 245.
54. O. M. J. van 't Erve, A. L. Friedman, CobasE, C. H. Li, J. T. Robinson and B. T. Jonker, *Nature Nanotech.*, 2012, 7, 737-742.
55. Y. Ando, K. Kasahara, S. Yamada, Y. Maeda, K. Masaki, Y. Hoshi, K. Sawano, M. Miyao and K. Hamaya, *Phys. Rev. B*, 2012, 85, 035320.
56. A. Jain, L. Louahadj, J. Peiro, J. C. L. Breton, C. Vergnaud, A. Barski, C. Beigné, L. Notin, A. Marty, V. Baltz, S. Auffret, E. Augendre, H. Jaffrès, J. M. George and M. Jamet, *Appl. Phys. Lett.*, 2011, 99, 162102.
57. S. Jahangir, F. Doğan, H. Kum, A. Manchon and P. Bhattacharya, *Phys. Rev. B*, 2012, 86, 035315.
58. M. Ramsteiner, H. Y. Hao, A. Kawaharazuka, H. J. Zhu, M. Kästner, R. Hey, L. Däweritz, H. T. Grahn and K. H. Ploog, *Phys. Rev. B*, 2002, 66, 081304.
59. H. C. Koo, H. Yi, J.-B. Ko, J. Chang, S.-H. Han, D. Jung, S.-G. Huh and J. Eom, *Appl. Phys. Lett.*, 2007, 90, 022101.
60. K. L. Litvinenko, L. Nikzad, J. Allam, B. N. Murdin, C. R. Pidgeon, J. J. Harris, T. Zhang and L. F. Cohen, *J. Appl. Phys.*, 2007, 101, 083105.
61. Y. Yafet, in *Solid State Phys.*, eds. S. Frederick and T. David, Academic Press, 1963, vol. 14, pp. 1-98.
62. F. J. Jedema, M. S. Nijboer, A. T. Filip and B. J. van Wees, *Phys. Rev. B*, 2003, 67, 085319.
63. R. J. Elliott, *Phys. Rev.*, 1954, 96, 266.
64. P. R. Hammar and M. Johnson, *Phys. Rev. Lett.*, 2002, 88, 066806.
65. P. R. Hammar, B. R. Bennett, M. J. Yang and M. Johnson, *Phys. Rev. Lett.*, 1999, 83, 203.
66. M. Oltcher, M. Ciorga, M. Utz, D. Schuh, D. Bougeard and D. Weiss, *Phys. Rev. Lett.*, 2014, 113, 236602.
67. F. Pezzoli, F. Bottegoni, D. Trivedi, F. Ciccacci, A. Giorgioni, P. Li, S. Cecchi, E. Grilli, Y. Song, M. Guzzi, H. Dery and G. Isella, *Phys. Rev. Lett.*, 2012, 108, 156603.
68. A. A. Balandin, *J. Nanosci. Nanotechnol.*, 2005, 5, 1015-1022.
69. A. W. Holleitner, V. Sih, R. C. Myers, A. C. Gossard and D. D. Awschalom, *Phys. Rev. Lett.*, 2006, 97, 036805.
70. S. Kettemann, *Phys. Rev. Lett.*, 2007, 98, 176808.
71. S. Patibandla, S. Pramanik, S. Bandyopadhyay and G. C. Tepper, *J. Appl. Phys.*, 2006, 100, 044303.
72. Th. Schäfers, V. A. Guzenko, M. G. Pala, U. Zülicke, M. Governale, J. Knobbe and H. Hardtdegen, *Phys. Rev. B*, 2006, 74, 081301.
73. A. E. Hansen, M. T. Björk, C. Fasth, C. Thelander and L. Samuelson, *Phys. Rev. B*, 2005, 71, 205328.
74. P. Roulleau, T. Choi, S. Riedi, T. Heinzel, I. Shorubalko, T. Ihn and K. Ensslin, *Phys. Rev. B*, 2010, 81, 155449.
75. S. M. George, *Chem. Rev.*, 2009, 110, 111-131.
76. J. Tang, C.-Y. Wang, F. Xiu, Y. Zhou, L.-J. Chen and K. L. Wang, *Adv. Mater. Sci. Eng.*, 2011, 2011, 316513.
77. T. Wei, N. Binh-Minh, C. Renjie and A. D. Shadi, *Semicond. Sci. Technol.*, 2014, 29, 054004.
78. J. Tang, C.-Y. Wang, L.-J. Chen and K. L. Wang, *Nanotechnology (IEEE-NANO), 2012 12th IEEE Conference on*, 2012, 1-5.
79. S. Pramanik, C. G. Stefanita, S. Patibandla, S. Bandyopadhyay, K. Garre, N. Harth and M. Cahay, *Nature Nanotech.*, 2007, 2, 216-219.
80. Z. H. Xiong, D. Wu, Z. Vally Vardeny and J. Shi, *Nature*, 2004, 427, 821-824.
81. J. Tang, C.-Y. Wang, W. Jiang, L.-T. Chang, Y. Fan, M. Chan, C. Wu, M.-H. Hung, P.-H. Liu, H.-J. Yang, H.-Y. Tuan, L.-J. Chen and K. L. Wang, *Nano Lett.*, 2012, 12, 6372-6379.
82. M. Julliere, *Phys. Lett. A*, 1975, 54, 225-226.
83. L. J. Lauhon, M. S. Gudiksen, D. Wang and C. M. Lieber, *Nature*, 2002, 420, 57-61.
84. W. Lu, J. Xiang, B. P. Timko, Y. Wu and C. M. Lieber, *Proc. Natl. Acad. Sci.*, 2005, 102, 10046-10051.
85. J. Noborisaka, J. Motohisa, S. Hara and T. Fukui, *Appl. Phys. Lett.*, 2005, 87, 093109.
86. J. Tang, L.-T. Chang, X. Kou, K. Murata, E. S. Choi, M. Lang, Y. Fan, Y. Jiang, M. Montazeri, W. Jiang, Y. Wang, L. He and K. L. Wang, *Nano Lett.*, 2014, 14, 5423-5429.
87. A. Hirohata and K. Takanashi, *J. Phys. D: Appl. Phys.*, 2014, 47, 193001.
88. B. Behin-Aein, D. Datta, S. Salahuddin and S. Datta, *Nature Nanotech.*, 2010, 5, 266-270.

-
89. F. Xiu, Y. Wang, J. Kim, A. Hong, J. Tang, A. P. Jacob, J. Zou and K. L. Wang, *Nature Mater.*, 2010, 9, 337-344.
 90. D. E. Nikonov and G. I. Bourianoff, *IEEE Trans. Nanotech.*, 2005, 4, 206-214.

5